

First-order Reversal Curve Analysis of Phase Transitions in Electrochemical Adsorption: A New Experimental Technique Suggested by Computer Simulations

L. Abou Hamad^{1,2}, D.T. Robb², P.A. Rikvold^{1,2,3}

¹*Center for Materials Research and Technology and Department of Physics, Florida State University, Tallahassee, FL 32306-4350, USA*

²*School of Computational Science, Florida State University, Tallahassee, FL 32306-4120, USA*

³*National High Magnetic Field Laboratory, Tallahassee, FL 32310*

June 3, 2018

Abstract

The first-order reversal curve (FORC) method for analysis of systems undergoing hysteresis is applied to dynamical models of electrochemical adsorption. In this setting, the method can not only differentiate between discontinuous and continuous phase transitions, but can also quite accurately recover equilibrium behavior from dynamic analysis for systems with a continuous phase transition. Discontinuous and continuous phase transitions in a two-dimensional lattice-gas model are compared using the FORC method. The FORC diagram for a discontinuous phase transition is characterized by a negative (unstable) region separating two positive (stable) regions, while such a negative region does not exist for continuous phase transitions. Experimental data for FORC analysis could easily be obtained by simple reprogramming of a potentiostat designed for cyclic-voltammetry experiments.

Keywords: First-order Reversal Curve; Hysteresis; Continuous phase transition; Discontinuous phase transition; Lattice-gas model; Monte Carlo simulation; Cyclic-voltammetry experiments.

1 Introduction

Recent technological developments in electrochemical deposition have made possible experimental studies of atomic-scale dynamics [1]. It is therefore now both timely and important to develop new computational methods for the analysis of experimental adsorption dynamics. In this paper we apply one such analysis technique, the first-order reversal curve (FORC) method, to analyze model systems with continuous and discontinuous phase transitions. We propose that the method can be a useful new experimental tool in surface electrochemistry.

The FORC method was originally conceived [2] in connection with the Preisach model of magnetic hysteresis. It has since been applied to a variety of magnetic systems, ranging from magnetic recording media and nanostructures to geomagnetic compounds, undergoing *rate-independent* (i.e., very slow) magnetization reversal [3]. Recently, there have also been several FORC studies of *rate-dependent* reversal [4, 5, 6]. Here we introduce and apply the FORC method in an electrochemical context. For completeness, a brief translation to magnetic language is found in the Appendix.

We apply FORC analysis to rate-dependent adsorption in two-dimensional lattice-gas models of electrochemical deposition. Specifically, we study a lattice-gas model with attractive nearest-neighbor interactions (a simple model of underpotential deposition, UPD), being driven across its discontinuous phase transition by a time-varying electrochemical potential. In addition, we consider a lattice-gas model with repulsive lateral interactions and nearest-neighbor exclusion (similar to the model of halide adsorption on Ag(100), described in Refs. [7, 8, 9, 10]), being similarly driven across its continuous phase transition.

The rest of this paper is organized as follows. In Sec. 2 the FORC method is explained. The model used for both systems with continuous and discontinuous transitions is briefly discussed in Sec. 3. In Sec. 4 the dynamics of systems with a discontinuous phase transition are studied using Kinetic Monte Carlo (KMC) simulations, as well as a mean-field model. The dynamics of systems with a continuous phase transition are studied in Sec. 5. Finally, a comparison between the two kinds of phase transitions and our conclusions are presented in Sec. 6.

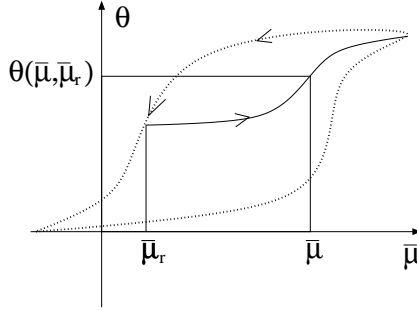


Figure 1: Schematic diagram of a FORC curve.

2 The FORC Method

For an electrochemical adsorption system, the FORC method consists of saturating the adsorbate coverage θ in a strong positive (for anions; negative for cations) electrochemical potential (proportional to the electrode potential) and, in each case starting from saturation, decreasing the potential to a series of progressively more negative ‘reversal potentials’ $\bar{\mu}_r$ (Fig. 1). Subsequently, the potential is increased back to the saturating value [3]. It is thus a simple generalization of the standard cyclic voltammetry (CV) method, in which the negative return potential is decreased for each cycle. This produces a family of FORCs, $\theta(\bar{\mu}_r, \bar{\mu})$, where θ is the adsorbate coverage, and where $\bar{\mu}$ is the instantaneous potential during the increase back toward saturation. Although we shall not discuss this further here, it is of course also possible to fix the negative limiting electrode potential and change the positive return potential from cycle to cycle.

It is further useful to calculate the FORC distribution,

$$\rho = -\frac{1}{2} \frac{\partial^2 \theta}{\partial \bar{\mu}_r \partial \bar{\mu}}, \quad (1)$$

which measures the sensitivity of the dynamics to the progress of reversal along the major loop.¹ The FORC distribution is usually displayed as a contour plot called a ‘FORC diagram.’ A positive value of ρ indicates that

¹Note that to normalize the FORC distribution, the term $\frac{1}{2} \delta(\bar{\mu} - \bar{\mu}_r) \frac{\partial \theta(\bar{\mu}_r, \bar{\mu})}{\partial \bar{\mu}}|_{\bar{\mu} \rightarrow \bar{\mu}_r^+}$ must be added to Eq. (1) [11]. Here we consider the distribution only away from the line $\bar{\mu} = \bar{\mu}_r$. The additional term could be found from the major loop.

the corresponding reversal curves are converging with increasing $\bar{\mu}$, while a negative value indicates divergence. Some preliminary results of this work have been submitted for publication elsewhere [12].

3 Model

KMC simulations of lattice-gas models, where a Monte Carlo (MC) step corresponds to an attempt to cross a free-energy barrier, have been used to simulate the kinetics of electrochemical systems with discontinuous [9, 10, 13, 14] or continuous [7, 15] phase transitions in two dimensions. The energy associated with a lattice-gas configuration is described by the grand-canonical effective Hamiltonian for an $L \times L$ square system of adsorption sites,

$$\mathcal{H} = - \sum_{i < j} \phi_{ij} c_i c_j - \bar{\mu} \sum_{i=1}^{L^2} c_i , \quad (2)$$

where $\sum_{i < j}$ is a sum over all pairs of sites, ϕ_{ij} are the lateral interaction energies between particles on the i th and j th sites measured in meV/pair, and $\bar{\mu}$ is the electrochemical potential measured in meV/atom. The local occupation variables c_i can take the values 1 or 0, depending on whether site i is occupied by an ion (1) or solvated (0). The sign convention is chosen such that $\bar{\mu} > 0$ favors adsorption, and negative values of ϕ_{ij} denote repulsion while positive values denote attraction between adsorbate particles on the surface. In addition to adsorption/desorption steps, we include diffusion steps with a comparable free-energy barrier [7].

In each time step of the KMC simulation, an adsorption site is chosen at random and the transition rates from the present configuration to a set of new configurations (desorption, diffusion) are calculated. A weighted list for accepting each of these moves is constructed using Eq. (4) below, to calculate the probabilities $R(F|I)$ of the individual moves between the initial state I and final state F . The probability for the system to stay in the initial configuration is consequently $R(I|I) = 1 - \sum_{F \neq I} R(F|I)$ [7, 8].

Using a thermally activated, stochastic barrier-hopping picture, the energy of the transition state for a microscopic change from an initial state I to a final state F is approximated by the symmetric Butler-Volmer formula [16, 17, 18]

$$U_{T_\lambda} = \frac{U_I + U_F}{2} + \Delta_\lambda . \quad (3)$$

Here U_I and U_F are the energies of the initial and final states, respectively, T_λ is the transition state for process λ , and Δ_λ is a “bare” barrier associated with process λ . This process can here be either nearest-neighbor diffusion (Δ_{nn}), next-nearest-neighbor diffusion (Δ_{nnn}), or adsorption/desorption ($\Delta_{a/d}$). The probability for a particle to make a transition from state I to state F is approximated by the one-step Arrhenius rate [16, 17, 18]

$$\mathcal{R}(F|I) = \nu \exp\left(-\frac{(U_{T_\lambda} - U_I)}{k_B T}\right) = \nu \exp\left(-\frac{\Delta_\lambda}{k_B T}\right) \exp\left(-\frac{U_F - U_I}{2k_B T}\right), \quad (4)$$

where ν is the attempt frequency, which sets the overall timescale for the simulation. The electrochemical potential $\bar{\mu}$, which is proportional to the electrode potential, is increased monotonically, preventing the system from reaching equilibrium at the instantaneous value of $\bar{\mu}$.

Independent of the diffusional degree of freedom, attractive interactions ($\phi_{ij} > 0$) produce a discontinuous phase transition between a low-coverage phase at low $\bar{\mu}$, and a high-coverage phase at high $\bar{\mu}$. In contrast, repulsive interactions ($\phi_{ij} < 0$) produce a continuous phase transition between a low-coverage disordered phase for low $\bar{\mu}$, and a high-coverage, ordered phase for high $\bar{\mu}$. Examples of systems with a discontinuous phase transition include underpotential deposition [13, 14, 19], while the adsorption of halides on Ag(100) [7, 8, 15, 20, 21] are examples of systems with a continuous phase transition.

4 Discontinuous Phase Transition

A two-dimensional lattice gas with attractive adsorbate-adsorbate lateral interactions that cause a discontinuous phase transition is a simple model of electrochemical underpotential deposition [13, 14, 19, 22]. Using a lattice-gas model with attractive interactions on an $L \times L$ lattice with $L = 128$, a family of FORCs were simulated, averaging over ten realizations for each reversal curve at room temperature. The lateral interaction energy (restricted to nearest-neighbor) was taken to be $\phi_{ij} = \phi_{nn} = 55$ meV, where the positive value indicates nearest-neighbor attraction. For this value of ϕ_{nn} , room temperature corresponds to $T = 0.8T_c$, where T_c is the critical temperature. The barriers for adsorption/desorption and diffusion (nearest-neighbor only) were $\Delta_{a/d} = \Delta_{nn} = 150$ meV, corresponding to relatively slow diffusion [14].

Simulation runs with faster diffusion ($\Delta_{nn} = 125$ meV) and the same adsorption/desorption barrier showed little difference from Fig. 2, indicating that diffusion effects are not significant for this model. The reversal electrochemical potentials $\bar{\mu}_r$ associated with the reversal curves were separated by 1 meV increments in the interval $[-200 \text{ meV}, 0 \text{ meV}]$, and the field-sweep rate was constant at $|\text{d}\bar{\mu}/\text{d}t| = 0.3 \text{ meV/MCSS}$. The FORCs are shown in Fig. 2(a), with a vertical line indicating the position of the coexistence value of the electrochemical potential, $\bar{\mu}_0 = -110 \text{ meV}$, and circles showing the position of the minimum of each FORC.

In a simple Avrami's-law analysis, the FORC minima all lie at $\bar{\mu} = \bar{\mu}_0$ [6]. However, in the simulations the minima are displaced. For $\theta > 0.5$, the minima occur at $\bar{\mu} < \bar{\mu}_0$, precisely at the points where the tendency to phase order, which drives local regions of the system toward the nearby metastable state ($\theta \approx 1$), is momentarily balanced by the electrochemical potential, which drives the system toward the distant stable state ($\theta \approx 0$). For $\theta < 0.5$, the stable and metastable states are $\theta \approx 1$ and $\theta \approx 0$, respectively, and the same balancing effect explains the FORC minima occurring at $\bar{\mu} > \bar{\mu}_0$.

The net effect is a 'back-bending' of the curve of minima, as seen in Fig. 2(a). The definition in Eq. (1) implies that the FORC distribution ρ should be negative in the vicinity of the back-bending. This can be seen in Fig 2(b), where the FORC distribution is plotted against the variables $\bar{\mu}_b = (\bar{\mu}_r + \bar{\mu})/2$ and $\bar{\mu}_c = (\bar{\mu}_r - \bar{\mu})/2$. The negative values of ρ reflect a local divergence of the FORCs away from each other, which can be considered a dynamical instability, caused by the competition between the tendency to phase order and the effect of the electrochemical potential. It is important to note that, when the potential sweep is stopped suddenly, after the dynamical instability played out on short timescales, the system is observed to relax reliably to the stable state at that potential on large timescales. The only exception is the point $(\bar{\mu} = \bar{\mu}_0, \theta = 0.5)$ along the FORC indicated by a bold line in Figs. 2(a) and 2(b). It is also interesting to note that the curve connecting the minima of the FORCs resembles the van der Waals loop in the mean-field isotherm of a fluid system [25], but with an asymmetrical shape about the point $(\bar{\mu} = \bar{\mu}_0, \theta = 0.5)$ and with a sweep-rate dependent shape (see Fig. 3).

We next explore this connection with the van der Waals loop in numerical solutions of a kinetic mean-field model. We can describe the competition between the phase-ordering and the influence of the potential explicitly, using a time-dependent mean-field model of the dynamics. The free energy is

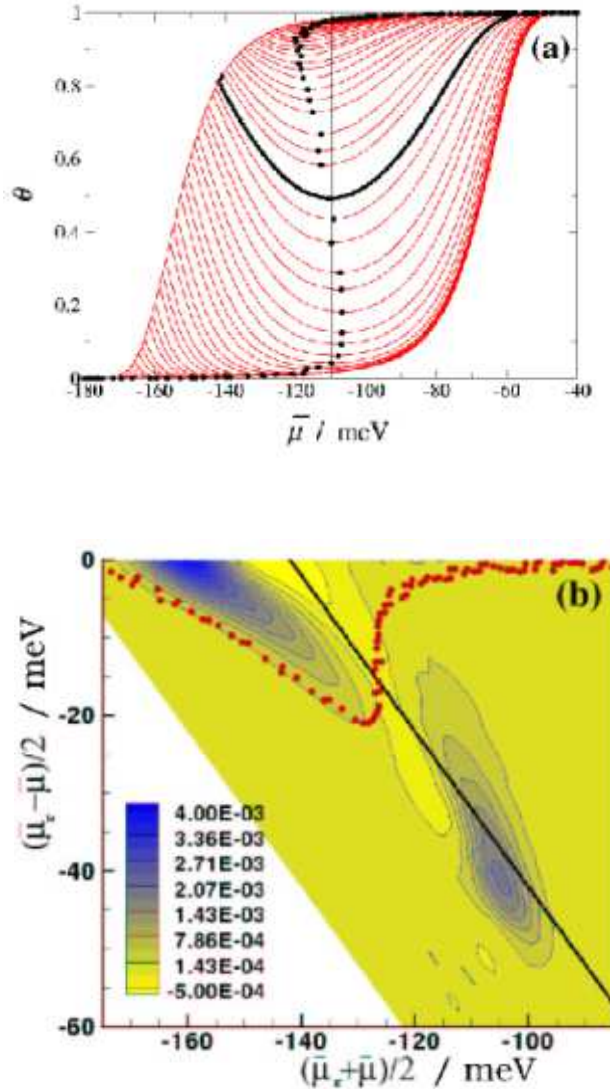


Figure 2: (Color online.) First-order reversal curves (FORCs) for a discontinuous phase transition. The vertical line shows the position of the coexistence value, $\bar{\mu} = \bar{\mu}_0$. The minima of each FORC are also shown (circles). (b) FORC diagram generated from the family of FORCs shown in (a). The positions of the FORC minima are also shown (circles). The straight line corresponds to the FORC for which the minimum lies at the coexistence value $\bar{\mu} = \bar{\mu}_0$ (thick curve in (a)). After Ref. [12].

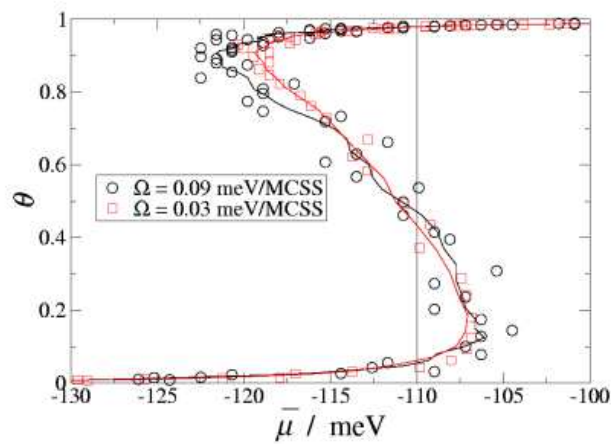


Figure 3: FORC minima dependence on sweep rate. The figure shows FORC minima for two families of FORCs with different sweep rates ($\Omega = 0.03$ and 0.09 meV/MCSS). The lines are guides to the eye, obtained by smoothing the data using a Savitzky-Golay method [23, 24] with a first-order polynomial and a window of 5 points.

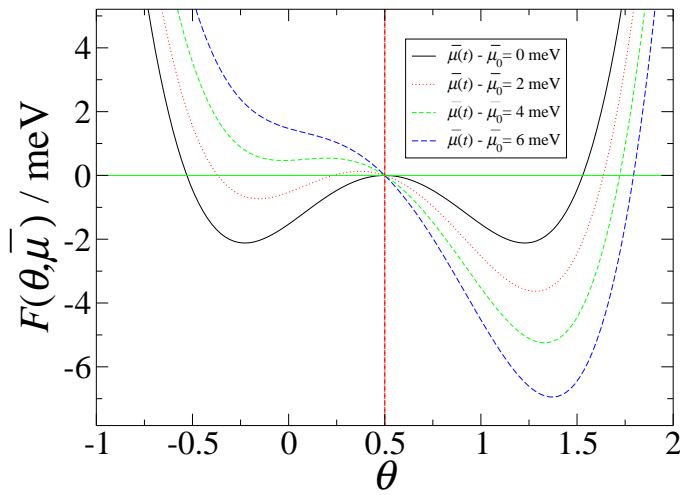


Figure 4: (Color online.) Free energy of a fourth-order Ginzburg-Landau form as a function of θ , given by Eq. (5). The parameters were calculated as $a = 30.2$ meV, $b = 16.0$ meV, $\theta_c = 0.5$, and $(\bar{\mu} - \bar{\mu}_0) = 0, 2, 4$, and 6 meV. A metastable state at $\theta < 0.5$ exists for the curves with $(\bar{\mu} - \bar{\mu}_0) = 0, 2, 4$ meV, but has disappeared in the curve $(\bar{\mu} - \bar{\mu}_0) = 6$ meV. The metastable minimum disappears at the so-called spinodal potential, $\bar{\mu}_{\text{sp}} - \bar{\mu}_0 = \frac{2b}{3} \sqrt{\frac{b}{3a}} \approx 4.48$ meV.

approximated by a fourth-order Ginzburg-Landau form [26],

$$F(\theta, \bar{\mu}(t)) = a \frac{(\theta - \theta_c)^4}{4} - b \frac{(\theta - \theta_c)^2}{2} - (\theta - \theta_c)(\bar{\mu}(t) - \bar{\mu}_0). \quad (5)$$

A plot of Eq. (5) is shown in Fig. 4 for $\theta_c = 0.5$, with the values of a and b calculated as described below and with $\bar{\mu}(t) - \bar{\mu}_0 = 0, 2, 4$, and 6 meV . In the noise-free (zero-temperature) case, the dynamics are given by

$$\frac{d\theta}{dt} = -\frac{1}{\gamma} \frac{\partial F}{\partial \theta} = -\frac{1}{\gamma} \left(a(\theta - \theta_c)^3 - b(\theta - \theta_c) - (\bar{\mu}(t) - \bar{\mu}_0) \right), \quad (6)$$

where γ is a phenomenological damping parameter. The parameters to use in this mean-field model can be determined directly from the simulated family of FORCs. On the curve of minima of the FORCs, $d\theta/dt = 0$, which implies

$$a(\theta - \theta_c)^3 - b(\theta - \theta_c) - (\bar{\mu} - \bar{\mu}_0) = 0. \quad (7)$$

Differentiating with respect to $\bar{\mu}$ and solving for $d\theta/d\bar{\mu}$ gives

$$\frac{d\theta}{d\bar{\mu}} = \frac{1}{3a(\theta - \theta_c)^2 - b}. \quad (8)$$

For $\theta = \theta_c$, this yields $b = - (d\theta/d\bar{\mu}|_{\theta=\theta_c})^{-1}$. The so-called spinodal potential $\bar{\mu}_{\text{sp}}$, and spinodal coverage θ_{sp} , occur where $d\theta/d\bar{\mu}$ diverges, so that

$$3a(\theta_{\text{sp}} - \theta_c)^2 - b = 0, \quad (9)$$

yielding

$$a = b/[3(\theta_{\text{sp}} - \theta_c)^2]. \quad (10)$$

The damping parameter γ can be related to the “coercive potential” $\bar{\mu}_{\text{coer}}$ (The value of the electrochemical potential at which $\theta = \theta_c$ on the major loop), the slope $\frac{d\theta}{d\bar{\mu}}|_{\bar{\mu}=\bar{\mu}_{\text{coer}}}$, and the sweep rate $d\bar{\mu}/dt$ as

$$\left. \frac{d\theta}{d\bar{\mu}} \right|_{\bar{\mu}=\bar{\mu}_{\text{coer}}} = \frac{d\theta/dt|_{\theta=\theta_c}}{d\bar{\mu}/dt} = \frac{(\bar{\mu}_{\text{coer}} - \bar{\mu}_0)}{\gamma d\bar{\mu}/dt}, \quad (11)$$

where we have used Eq. (6) in the last step.

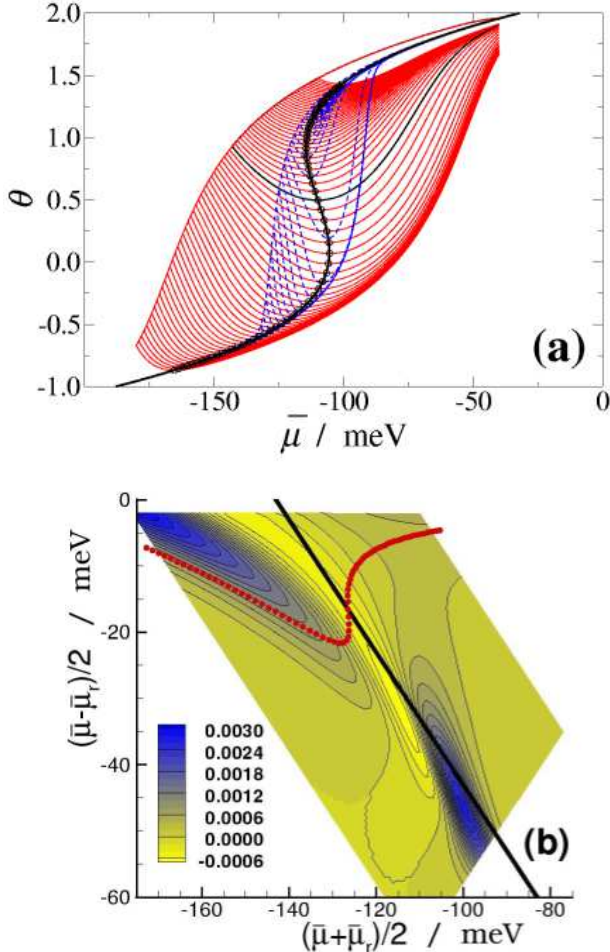


Figure 5: (Color online.) Reversal behavior of a dynamic mean-field model: (a) Families of FORCs. (b) FORC distribution for one family. The parameters were calculated as $a = 30.2$ meV, $b = 16.0$ meV, and $\gamma = 3720$ MCSS meV to fit the results of Fig. 2(a). In (a), the solid lines show the FORCs for faster sweep rate ($\Omega = 0.3$ meV/MCSS), and the dashed lines show the FORCs for a slower sweep rate ($\Omega = 0.03$ meV/MCSS). The thick line is the analytical result, Eq. (7), for the line of minima, while the circles show the actual minima from the numerical integration. In (b), the full FORC distribution is plotted vs $(\bar{\mu}_b, \bar{\mu}_c)$ (see text) for the FORCs with the faster sweep rate ($\Omega = 0.3$ meV/MCSS). The straight line corresponds to the FORC for which the minimum lies at the coexistence value $\bar{\mu} = \bar{\mu}_0$ (thick curve in (a)). The appearance is similar to Fig 2(b).

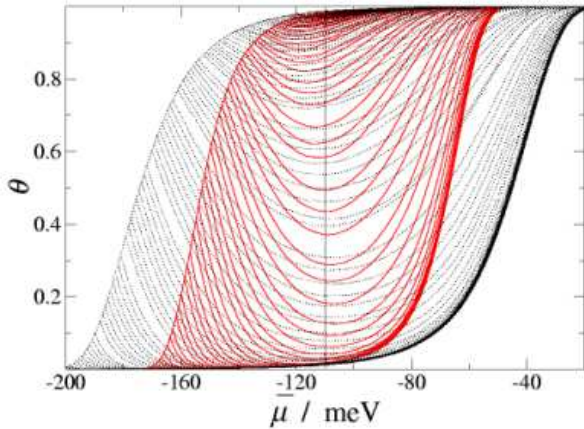


Figure 6: (Color online.) KMC simulation results for FORCs with different sweep rates, $\Omega = 0.03 \text{ meV/MCSS}$ (solid lines) and 0.09 meV/MCSS (dotted lines). The vertical line shows the coexistence value, $\bar{\mu} = \bar{\mu}_0$. The coercive potential for the FORCs with the slower sweep rate is shifted toward the $\bar{\mu} = \bar{\mu}_0$ line.

In Fig. 5(a), we show the family of FORCs obtained by numerical integration of the mean-field model, with parameters determined by a fit to the simulated family of FORCs in Fig. 2(a). The line of minima in Fig. 5(a) follows the analytical curve defined by Eq. (7), as expected. However, in contrast to Fig. 2(a), the line of minima is symmetric about the point $(\bar{\mu} = \bar{\mu}_0, \theta = \theta_c)$. In addition, in KMC simulations at a slower sweep rate, we found that both the coercive potential (Fig. 6) and the line of minima (Fig. 3) of the FORCs were shifted toward $\bar{\mu} = \bar{\mu}_0$. In contrast, in the mean-field model at a slower sweep rate, the coercive field decreases, but the line of minima remains unchanged (as it must, since Eq. (7) is independent of the sweep rate). Preliminary simulations indicate that including thermal noise in the mean-field model may further improve the agreement with the MC results.

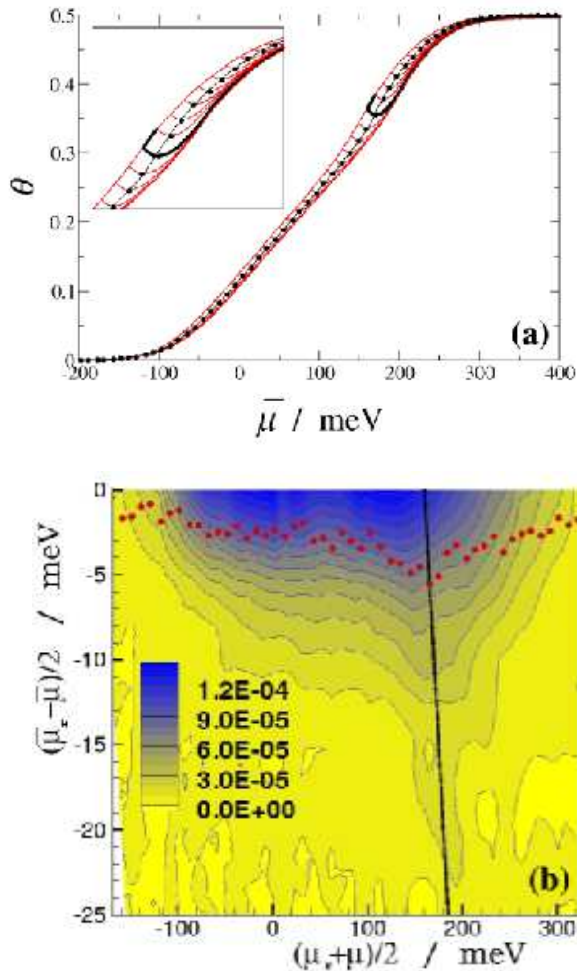


Figure 7: (Color online.) (a) First-order reversal curves (FORCs) for a continuous phase transition simulated at a slow scan rate $\Omega = 0.0003$ meV/MCSS. The thin black middle line shows the equilibrium curve. The inset is a magnification of the critical region. The minima of each FORC are also shown (black filled circles). The thick black line shows the first FORC which dips below the critical coverage. (b) FORC diagram generated from the FORCs shown in (a). The positions of the FORC minima are also shown (circles). The straight line corresponds to the first FORC for which the minimum dips below the critical coverage. After Ref. [12].

5 Continuous Phase Transition

Using the same Hamiltonian, but with long-range repulsive interactions and nearest-neighbor exclusion as discussed in Ref. [7], KMC simulations were used to produce the family of FORCs for a continuous phase transition. The reversal potentials $\bar{\mu}_r$ were separated by 10 meV increments in the interval $[-200 \text{ meV}, 400 \text{ meV}]$. As in Ref. [7], the repulsive $1/r^3$ interactions, with nearest-neighbor exclusion and $\phi_{\text{nnn}} = -21 \text{ meV}$, are calculated with exact contributions for $r_{ij} \leq 3$, and using a mean-field approximation for $r_{ij} > 3$. The barriers for adsorption/desorption and nearest- and next-nearest-neighbor diffusion, are $\Delta_{\text{a/d}} = 300 \text{ meV}$, $\Delta_{\text{nn}} = 100 \text{ meV}$, and $\Delta_{\text{nnn}} = 200 \text{ meV}$, respectively [7]. Larger values of the diffusion barrier were also used to study the effect of diffusion on the dynamics. A continuous phase transition occurs between a disordered state at low coverage and an ordered state at high coverage [20, 21]. The FORCs and the FORC diagram are shown in Fig. 7. Also indicated in Fig. 7(a) are the FORC minima and the equilibrium isotherm.

Note that the FORC minima in Fig. 7(a) lie directly on the equilibrium isotherm. This is because such a system has one stable state for any given value of the potential, as defined by the continuous equilibrium curve. The uniformly positive value of the FORC distribution in Fig. 7(b) reflects the convergence of the family of FORCs with increasing $\bar{\mu}$. This convergence results from relaxation toward the equilibrium isotherm, at a rate which increases with the distance from equilibrium. It is interesting to note that, while it is difficult to see at this slow scan rate, the rate of approach to equilibrium decreases greatly along the first FORC that dips below the critical coverage $\theta_c \approx 0.36$ (shown in bold in Fig. 7(a)). The FORCs that lie completely in the range $\theta > 0.36$ never enter into the disordered phase, and thus their approach to equilibrium is not hindered by jamming. This is a phenomenon that occurs when further adsorption in a disordered adlayer is hindered by the nearest-neighbor exclusion. As a result, extra diffusion steps are needed to make room for the new adsorbates, and the system follows different dynamics than a system with an ordered adlayer [27]. The FORCs that dip below $\theta_c = 0.36$ enter into the disordered phase, and thus their approach to equilibrium is delayed by jamming. This is reflected in the FORC diagram by the Florida-shaped “peninsula” centered around this FORC in Fig. 7(b).

The effect of jamming is more pronounced at higher scan rates, or with

a higher diffusion barrier, where the rate of adsorption is much faster than the rate of diffusion. The family of FORCs and FORC diagram at a higher scan rate, $\Omega = 0.01$ meV/MCSS, are shown in Fig. 8, and the FORCs and FORC diagram with a larger diffusion barrier are shown in Fig. 9. In Fig. 8, two distinct groups of FORCs undergoing jammed and unjammed dynamics can be clearly seen. This is reflected in the FORC diagram as a splitting of the “peninsula” into two “islands” of high ρ values. A similar effect is seen in Fig. 9, since also there the rate of adsorption is much faster than the rate of diffusion (larger diffusion barrier). However, Fig. 9(a) shows a slight difference between the FORC minima and the equilibrium curve around the critical coverage. Notice also in Fig. 8(a) that even at a much higher scan rate than in Fig. 7 (nearly two orders of magnitude), the FORC minima still follow the equilibrium curve very accurately. Thus, the FORC method should be useful to obtain the equilibrium adsorption isotherm quite accurately in experimental systems with slow equilibration rates.

6 Comparison and conclusions

Two observations can be made by comparing the FORCs and FORC diagrams for systems with discontinuous and continuous phase transitions. First, the FORC minima in systems with a continuous phase transition correspond to the equilibrium behavior, while they do not for systems with a discontinuous phase transition. Thus, FORCs can be used to recover the equilibrium behavior for systems with continuous phase transitions that need a long time to equilibrate. This could be useful in experiments. Second, due to the instability that exists in systems with a discontinuous phase transition, the minima of the family of FORCs form a back-bending “van der Waals loop”, and the corresponding FORC diagram contains negative regions which do not exist for systems with a continuous phase transition. Since experimental implementation of the FORC method should only require simple reprogramming of a potentiostat designed to carry out a standard CV experiment, we believe the method can be of significant use in obtaining additional dynamic as well as equilibrium information from such experiments for systems that exhibit electrochemical adsorption with related phase transitions.

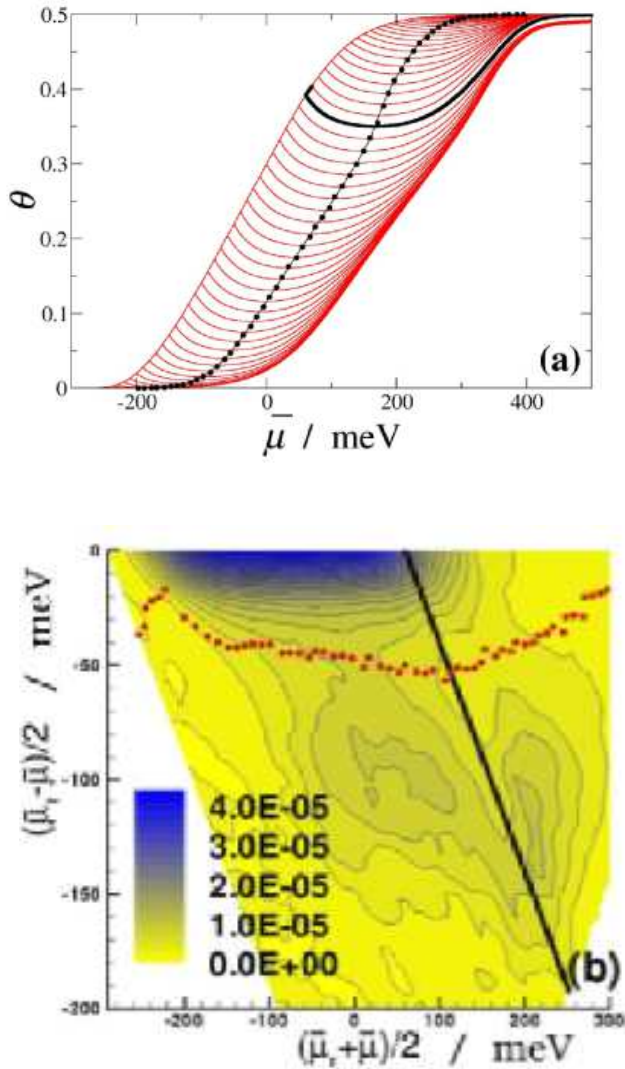


Figure 8: (Color online.) (a) First-order reversal curves (FORCs) for a continuous phase transition simulated at a high scan rate, $\Omega = 0.01$ meV/MCSS. The black curve in the middle shows the equilibrium isotherm. The minima of each FORC are also shown (black filled circles). (b) FORC distribution generated from the FORCs shown in (a). The positions of the FORC minima are also shown (black filled circles). The straight line corresponds to the FORC for which the minimum lies closest to the critical coverage.

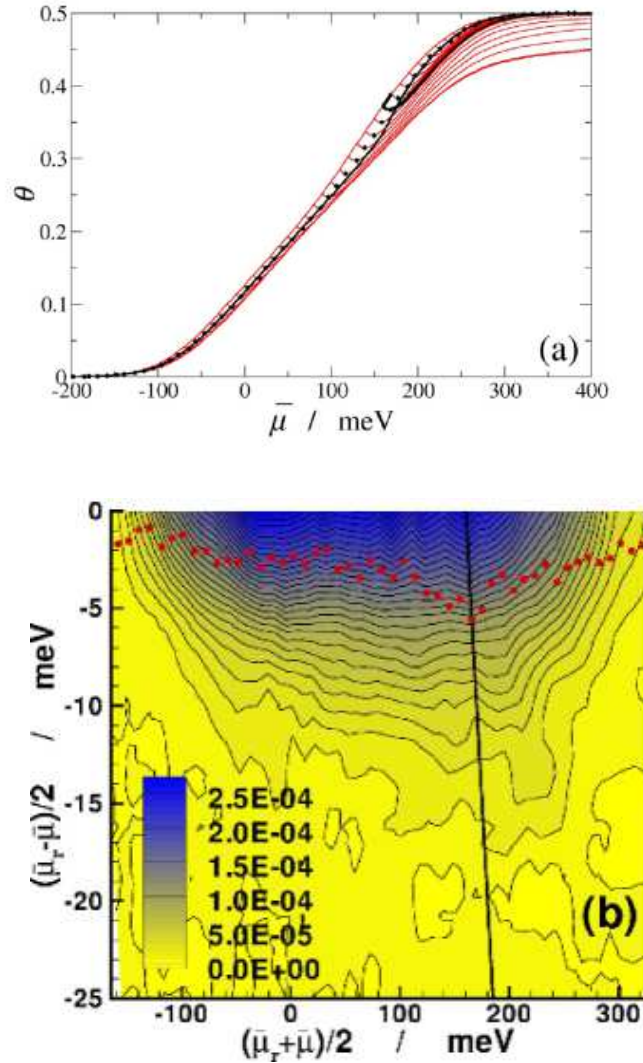


Figure 9: (Color online.) (a) First-order reversal curves (FORCs) for a continuous phase transition simulated with a large diffusion barrier $\Delta_{nn} = 300$ meV. The black curve in the middle shows the equilibrium isotherm. The minima of each FORC are also shown (black filled circles). (b) FORC distribution generated from the FORCs shown in (a). The positions of the FORC minima are also shown (black filled circles). The straight line corresponds to the FORC for which the minimum lies closest to the critical coverage.

Acknowledgments

This research was supported by U.S. NSF Grant No. DMR-0240078, and by Florida State University through the School of Computational Science, the Center for Materials Research and Technology, and the National High Magnetic Field Laboratory.

Appendix

In this appendix we present a mapping between lattice-gas models of adsorption and discrete spin models of magnetic systems, and then introduce the FORC method in the original magnetic language.

The occupation variable in the lattice-gas model, $c_i \in \{0, 1\}$ is a binary variable, just like the magnetization variables: $s_i = M_s/m_s \in \{-1, 1\}$ in the Classical Preisach Model (CPM). We therefore have the mappings $c_i = (s_i + 1)/2$ and $(\bar{\mu} - \bar{\mu}_0) = 2H$ [14, 28, 29]. As a result, the FORC method can be applied to electrochemical adsorption, as well as to magnetic hysteresis.

The CPM is based on the idea that a material consists of a number of elementary interacting “particles” or “domains,” called hysterons. The hysterons are assumed to have rectangular hysteresis loops between two states that have the same magnetization values, $+m_s$ and $-m_s$, for all hysterons. A typical hysteresis loop for a hysteron is shown in Fig. 10. H_u and H_d are the up and down switching magnetic fields respectively. It is also assumed that the different hysterons have a distribution of reversal fields $\Phi(H_u, H_d)$. In the CPM, the total magnetization can be defined as [30]

$$M(t) = \iint_{H_u \geq H_d} \Phi(H_u, H_d) [\hat{m}(H_u, H_d) H(t)] dH_u dH_d, \quad (12)$$

where the operator $\hat{m}(H_u, H_d)$ applied to $H(t)$ gives $+m_s$ if the particle is switched up and $-m_s$ if the particle is switched down. Note that $\hat{m}(H_u, H_d) H(t)$ depends on the field history of $H(t)$ and not only on the instantaneous value, which enables the CPM to model irreversible hysteresis behavior. For a detailed discussion of the Preisach Model, see Ref. [30].

In a typical FORC analysis of a magnetic system, the magnetization M is saturated in a positive applied magnetic field, and then the applied magnetic field is decreased continuously to a reversal field H_r . The magnetic field is then increased back to saturation. A first-order reversal curve is the response

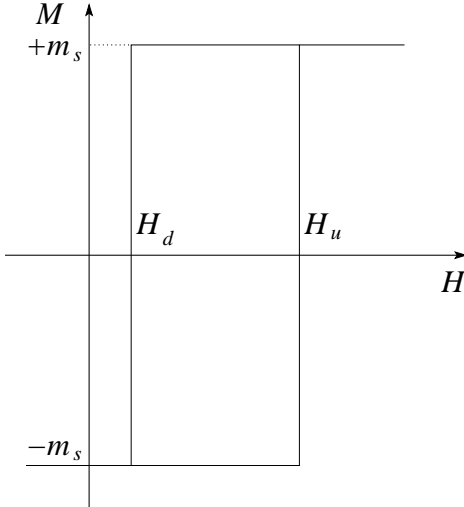


Figure 10: Schematic diagram of a hysteresis loop for a single hysteron. H_u and H_d are the up and down reversal fields, respectively. After Ref. [30].

of the magnetization to the increasing magnetic field ($H > H_r$). This is done for different values of H_r , and a set of curves, $M(H_r, H)$, is collected [3, 11]. The FORC distribution is defined as

$$\tilde{\rho} = -\frac{1}{2} \frac{\partial^2 M(H_r, H)}{\partial H_r \partial H}, \quad (13)$$

where the tilde denotes a trivially different normalization from the one used here. Thus, using the mapping given above, one arrives at Eq. (1) as the definition of the FORC distribution in an electrochemical system.

References

- [1] T. Tansel, O. M. Magnussen, Phys. Rev. Lett. 96 (2006) 026101.
- [2] I. D. Mayergoyz, IEEE Trans. Magn. MAG 22 (1986) 603.
- [3] C. R. Pike, A. P. Roberts, K. L. Verosub, J. Appl. Phys. 85 (1999) 6660.
- [4] C. Enachescu, R. Tanasa, A. Stancu, F. Varret, J. Linares, E. Codjovi, Phys. Rev. B 72 (2005) 054413.

- [5] M. Fecioru-Morariu, D. Ricinschi, P. Postolache, C. E. Ciomaga, A. Stancu, *J. Optoelectron. Adv. Mater.* 6 (2004) 1059.
- [6] D. T. Robb, M. A. Novotny, P. A. Rikvold, *J. Appl. Phys.* 97 (2005) 10E510.
- [7] I. Abou Hamad, P. A. Rikvold, G. Brown, *Surf. Sci.* 572 (2004) L355–L361.
- [8] S. J. Mitchell, G. Brown, P. A. Rikvold, *Surf. Sci.* 471 (2001) 125–142.
- [9] I. Abou Hamad, Th. Wandlowski, G. Brown, and P. A. Rikvold, *J. Electroanal. Chem.* 554-555 (2003) 211–219.
- [10] I. Abou Hamad, S. J. Mitchell, Th. Wandlowski, and P. A. Rikvold, *Electrochim. Acta* 50 (2005) 5518–5525.
- [11] C. R. Pike, *Phys. Rev. B* 68 (2003) 104424.
- [12] I. Abou Hamad, D. T. Robb, P. A. Rikvold, in: D. P. Landau, S. P. Lewis, H.-B. Schüttler (Eds.), *Computer Simulation Studies in Condensed-Matter Physics XIX*, Springer-Verlag, Berlin, in press.
- [13] S. Frank, D. E. Roberts, P. A. Rikvold, *J. Chem. Phys.* 122 (2005) 064705.
- [14] S. Frank, P. A. Rikvold, *Surf. Sci.*, in press.
- [15] S. J. Mitchell, S. Wang, P. A. Rikvold, Halide adsorption on single-crystal silver substrates: Dynamic simulations and *ab initio* density functional theory, *Faraday Disc.* 121 (2002) 53–69.
- [16] G. Brown, P. A. Rikvold, S. J. Mitchell, M. A. Novotny, in: A. Wieckowski (Ed.), *Interfacial Electrochemistry: Theory, Experiment, and Application*, Marcel Dekker, New York, 1999, pp. 47–61.
- [17] H. C. Kang, W. H. Weinberg, *J. Chem. Phys.* 90 (1989) 2824–2830.
- [18] G. M. Buendía, P. A. Rikvold, K. Park, M. A. Novotny, *J. Chem. Phys.* 121 (2004) 4193–4202.
- [19] G. Brown, P. A. Rikvold, M. A. Novotny, A. Wieckowski, *J. Electrochem. Soc.* 146 (1999) 1035.

- [20] B. M. Ocko, J. X. Wang, and Th. Wandlowski, Phys. Rev. Lett. 79 (1997) 1511–1514.
- [21] Th. Wandlowski, J. X. Wang, and B. M. Ocko, J. Electroanal. Chem. 500 (2001) 418–434.
- [22] R. A. Ramos, P. A. Rikvold, M. A. Novotny, Phys. Rev. B 59 (1999) 9053–9069.
- [23] A. Savitzky, M. J. E. Golay, Anal. Chem. 36 (1964) 1627–1639.
- [24] W. H. Press, A. Teukolsky, W. T. Vetterling, B. P. Flannery, Numerical Recipes in C: The Art of Scientific Computing, Cambridge University Press, Cambridge, 1997.
- [25] G. W. Castellan, Physical Chemistry, Addison-Wesley, Reading, MA, 1964.
- [26] D. P. Landau, K. Binder, A Guide to Monte Carlo Simulations in Statistical Physics, Cambridge University Press, Cambridge, 2000.
- [27] J.-S. Wand, P. Nielaba, V. Privman, Mod. Phys. Lett. B 7 (1993) 189.
- [28] R. K. Pathria, Statistical Mechanics, 2nd Edition, Butterworth Heinemann, Oxford, UK, 1996.
- [29] C. N. Yang, T. D. Lee, Phys. Rev. 87 (1952) 410.
- [30] I. D. Mayergoyz, Mathematical Models of Hysteresis, Springer-Verlag, New York, 1991.